INSTITUTE OF PHYSICS PUBLISHING SMART MATERIALS AND STRUCTURES
Smart Mater. Struct. **16** (2007) S39–S50 doi:10.1088/0964-1726/16/1/S05

A 1D rate-dependent viscous constitutive model for superelastic shape-memory alloys: formulation and comparison with experimental data

Ferdinando Auricchio[1,2,3], **Davide Fugazza**[1,2,5] **and Reginald DesRoches**[4]

[1] European School for Advanced Studies in Reduction of Seismic Risk (ROSE School), Pavia, Italy
[2] Dipartimento di Meccanica Strutturale, Università degli Studi di Pavia, Pavia, Italy
[3] Istituto di Matematica Applicata e Tecnologie Informatiche, Pavia, Italy
[4] School of Civil and Environmental Engineering, Georgia Institute of Technology, Atlanta, GA, USA

E-mail: davide.fugazza@samcef.com

Received 26 April 2005, in final form 8 May 2006
Published 15 January 2007
Online at stacks.iop.org/SMS/16/S39

Abstract
Experimental investigations on superelastic shape-memory alloys (SMAs) show a dependence of the stress–strain relationship on the loading–unloading rate. This feature is of particular importance when utilizing SMA materials for seismic applications, since the loading rate may affect the structural response.

Motivated by this observation and by the fact that there exist relatively few studies on the material modelling of SMAs in earthquake engineering, the present work addresses a uniaxial constitutive equation able to describe the rate-dependent behaviour of superelastic SMAs.

The formulation of the model is based on two scalar internal variables, the static martensite fraction and the dynamic martensite fraction, for which three different types of evolutionary equations in rate form are proposed. Moreover, the model takes into account the different elastic properties between austenite and martensite.

Finally, after discussing two possible approaches for the solution of the corresponding time-discrete framework, the ability of the model to simulate experimental data obtained from uniaxial tests performed on SMA wires and bars at frequency levels of excitation typical of earthquake engineering is assessed.

(Some figures in this article are in colour only in the electronic version)

1. Introduction

Shape-memory alloys (SMAs) are a class of solids showing properties not present in materials traditionally utilized in engineering. In fact, SMAs have the ability to undergo reversible micromechanical phase transitions by changing the crystallographic structure from an *austenitic* phase to a *martensitic* phase. This capacity results in two major features at the macroscopic level, which are the *superelastic effect* and the *shape-memory effect* [9].

Due to these unique characteristics, SMAs lend themselves to innovative applications in many scientific fields,

[5] Author to whom any correspondence should be addressed. Present address: SAMTECH Italia s.r.l., Via Giovanni Rasori 13, I-20145 Milano, Italy.

ranging from biomedical devices, such as stents or orthodontic archwires, to apparatus for the deployment and control of space structures, such as antennas and satellites.

Recent experimental and numerical investigations have also shown the possibility of using such materials as vibration control devices. In particular, they have been shown to be effective in improving the structural response of buildings and bridges subjected to earthquakes [6, 15, 18].

However, despite the large number of constitutive equations available in the literature, only relatively few studies deal with the material modelling under dynamic loading conditions and, specifically, under loading conditions experienced by civil engineering structures during a seismic event [4, 11, 12, 16, 17].

Hence, the present work proposes a constitutive equation able to describe the rate-dependent superelastic behaviour of SMAs for seismic applications.

At this stage, it is also very important to emphasize that the philosophy adopted in the development of the model is to try to capture the rate-dependent response of superelastic SMAs through a simple as possible approach. Specifically, the present paper explores the possibility of reproducing, within a degree of accuracy to be assessed, such a behaviour through the use of a viscous-like model.

As will be addressed in section 3, the mechanisms behind the dependence of the stress–strain relationship exhibited by SMAs on the loading rate can be explained to some extent by considering both thermo-mechanical aspects associated with the phase transitions experienced by the material during deformation processes and thermo-mechanical balances. Therefore, the use of a viscous-like model has its justification not on the basis of properly reproducing the internal material mechanisms but in simulating a somehow 'equivalent' macroscopic response.

Furthermore, the study of the actual and less empirical material response is the object of a different contribution [3], where a more complex thermo-mechanical constitutive equation is presented.

The model herein considered is based on two scalar internal variables, the static martensite fraction and the dynamic martensite fraction, for which three different types of evolutionary equations in rate form are proposed. Moreover, the model takes into account the different elastic properties between austenite and martensite.

Finally, after discussing two possible approaches for the solution of the corresponding time-discrete framework, the ability of the model to simulate experimental data obtained from uniaxial tests performed on SMA wires and bars at frequency levels of excitation typical of earthquake engineering is assessed [7, 8, 10].

2. Overview on the constitutive modelling of SMAs for seismic applications

In this section, we focus attention on the constitutive modelling of SMAs for seismic applications. Since SMA-based devices are traditionally used in earthquake engineering as a combination of wires or bars [6, 15, 18], emphasis is given only to uniaxial models. In particular, in the following we briefly review the constitutive laws [4, 11, 12, 16, 17] which seem to be the most popular for the simulation of seismic devices based on the SMA technology.

Bernardini and Brancaleoni [4] focus on a model able to simulate the rate- and temperature-dependent response of SMAs, which is utilized for predicting the seismic response of framed structures equipped with superelastic SMA braces. In the proposed equation, SMAs are represented as a mixture of two solid phases whose individual behaviour is modelled as a linear isotropic thermoelastic material.

Fugazza *et al* [11] consider a rate- and temperature-independent constitutive equation for SMAs for the evaluation of the seismic performance of steel frames equipped with superelastic SMA braces. The model, which is a modification of the one previously introduced by Auricchio and Sacco [1], is developed in the small deformation regime, requires a limited number of material parameters and is able to reproduce partial and complete phase transformation patterns.

Graesser and Cozzarelli [12] study a one-dimensional model capable of capturing both the superelastic effect and the martensitic hysteresis with their sub-loops due to partial transformation processes. Model drawbacks are the inability to predict the material behaviour after phase transition completion as well as the rate and temperature independence. Also, the different elastic properties between austenite and martensite are not taken into consideration.

Tamai *et al* [16] concentrate on a temperature-dependent model in which the phase transformation stress levels are depending on the value of the martensite fraction. The adopted kinetic rules are exponential and differ according to the phase transformation being experienced by the material. The constitutive law, which is used to predict the seismic response of SMA elements, is rate-independent and requires a large number of experimental data.

Wilde *et al* [17] propose an innovative isolation system for bridges made of SMA bars. They improve the Graesser and Cozzarelli model by introducing the possibility of describing the material behaviour also after phase transformation completion as well as by simulating a smooth transition between the elastic branch and the superelastic plateau. However, the model is still rate- and temperature-independent.

As is clear from the presented review, the constitutive equations nowadays adopted for describing the macroscopic behaviour of SMAs for seismic applications are, in general, rate-independent. Therefore, the main goal of this paper is to propose a material model able to simulate the actual dependence of SMA materials on the strain rate, in order to provide the structural engineer with a reliable and user-friendly tool for the design of superelastic seismic devices.

3. A rate-dependent viscous constitutive model for superelastic SMAs

In the following, after providing some comments on the nature of the SMAs' rate-dependent behaviour and after discussing possible modelling approaches, we present a uniaxial viscous constitutive equation able to capture some basic rate-dependent aspects of superelastic SMA materials in the small deformation regime.

3.1. Basic considerations on the rate-dependent behaviour of SMAs

To properly understand and explain the rate-dependent mechanical behaviour of SMAs, it is fundamental to recall some aspects relative to the phase transformations occurring in the material during deformation processes:

(i) both stress and temperature can act as equivalent driving forces for the phase transformations;
(ii) latent heat production or adsorption is always associated with such phase transformations. In particular, the conversion of austenite into martensite is an exothermic transformation while the conversion of martensite into austenite is an endothermic transformation.

As experimentally proved [5, 8, 14], the above listed aspects play a fundamental role in the mechanical behaviour of SMAs undergoing dynamic loadings.

In fact, at high strain rates, the heat generated during the forward transformation may not have enough time to be transferred to the surrounding environment (in order to reach a static thermal equilibrium), then causing an increase of the material temperature. Consequently, the stress threshold for the activation of the transformation may rise, producing at the same time an increase of the slope of the superelastic plateaus.

In conclusion, based on the previous considerations, it is possible to state that such a strong thermo-mechanical coupling may change the overall material response during fast loading conditions as a consequence of the progressive heating of the SMA material under study.

3.2. Choice of the modelling approach

A possible approach to the modelling of SMAs for seismic applications, is to couple a standard rate-independent equation for the description of the active phase transition with a thermal balance law. This approach has been investigated, for example, by Auricchio *et al* [3], where the considered model is based on a single scalar internal variable, the martensite fraction, for which three different rate-independent evolutionary equations in rate form are proposed. Next, such equations are coupled with a thermal balance equation, in order to take into account the presence of internal heat sources in the form of phase-transition latent heat and mechanical dissipation. Clearly, the resulting expressions consider the temperature as a primary independent variable, which is responsible for the rate-dependent nature of the model.

However, in the present paper we would like to explore a different way of modelling the rate-dependent behaviour of SMAs. More precisely, driven by the interest to simulate the structural behaviour of complex applications in the field of earthquake engineering, we wish to explore an easier approach (and less tightly related to physical phenomena experienced by the material during external solicitations), with the hope of reducing the complexity of the formulation while still obtaining a good description of the material response.

In particular, starting from [2], we do not explicitly consider the temperature as a variable of the model but we include a viscous term in the kinetic rules, which should be able to capture the rate-dependent behaviour of SMAs from a phenomenological macroscopic point of view.

3.3. Internal variables and phase transitions

The material crystallographic state is described through two scalar internal variables, the *static martensite fraction*, ξ_{ST}, and the *dynamic martensite fraction*, ξ. The former represents the martensite fraction which would be obtained under static loading conditions or, equivalently, for a very small ratio between the loading rate and a characteristic *material internal time*, τ. Accordingly, the possible differences between ξ_{ST} and ξ should model either the presence of rate effects in the phase transformations or their dependence on rate phenomena, such as heat exchanges with the surrounding or other transient thermal processes.

Consistently with the introduction of a static and a dynamic martensite fraction, we also introduce two different stresses, the *static stress*, σ_{ST}, and the *dynamic stress*, σ, the former representing the stress which would be obtained in the material for static loading conditions.

In terms of phase transformations, we assume to work with two processes: the conversion of austenite into martensite ($A \rightarrow S$) and the conversion of martensite into austenite ($S \rightarrow A$). For each one, we consider the possibility of choosing between three different types of kinetic rules, indicated as *linear*, *power* and *exponential*, in the following presented according to an increasing order of complexity. Clearly, we assume that the two evolutionary processes may produce variations of both the static and dynamic martensite fraction.

3.4. Kinetic rules

The kinetic rules govern the evolution in time of the martensite fraction and are expressed as first-order differential equations. In the following, for each rule we provide the corresponding evolutionary equations for both forward (autenite-to-martensite) and reverse (martensite-to-austenite) phase transformations. In the adopted notation, $|\cdot|$ denotes the absolute value and a superposed dot indicates a time derivative[6].

Conversion of austenite into martensite

$$\text{Linear} \begin{cases} \dot{\xi}_{ST} = -(1-\xi_{ST}) \dfrac{\dot{\overline{|\sigma_{ST}|}}}{|\sigma_{ST}| - \sigma^{AS}_{f,ST}} \mathcal{H}^{AS}_{ST} \\ \dot{\xi} = -(1-\xi) \dfrac{\dot{\overline{|\sigma|}}}{|\sigma| - \sigma^{AS}_{f}} \mathcal{H}^{AS} - \dfrac{\xi - \xi_{ST}}{\tau}\, \mathcal{H}_v \end{cases} \tag{1}$$

$$\text{Power} \begin{cases} \dot{\xi}_{ST} = -\pi^{AS}_{ST}(1-\xi_{ST}) \dfrac{\dot{\overline{|\sigma_{ST}|}}}{|\sigma_{ST}| - \sigma^{AS}_{f,ST}} \mathcal{H}^{AS}_{ST} \\ \dot{\xi} = -\pi^{AS}(1-\xi) \dfrac{\dot{\overline{|\sigma|}}}{|\sigma| - \sigma^{AS}_{f}} \mathcal{H}^{AS} - \dfrac{\xi - \xi_{ST}}{\tau}\, \mathcal{H}_v \end{cases} \tag{2}$$

[6] In particular, a superposed dot over a bar indicates that the whole quantity under the bar is derived.

$$\text{Exponential}\begin{cases}\dot{\xi}_{\mathrm{ST}}=\beta_{\mathrm{ST}}^{\mathrm{AS}}(1-\xi_{\mathrm{ST}})\dfrac{\dot{\overline{|\sigma_{\mathrm{ST}}|}}}{(|\sigma_{\mathrm{ST}}|-\sigma_{f,\mathrm{ST}}^{\mathrm{AS}})^2}\mathcal{H}_{\mathrm{ST}}^{\mathrm{AS}}\\ \dot{\xi}=\beta^{\mathrm{AS}}(1-\xi)\dfrac{\dot{\overline{|\sigma|}}}{(|\sigma|-\sigma_f^{\mathrm{AS}})^2}\mathcal{H}^{\mathrm{AS}}\\ \quad-\dfrac{\xi-\xi_{\mathrm{ST}}}{\tau}\,\mathcal{H}_v\end{cases}\tag{3}$$

where $\mathcal{H}_{\mathrm{ST}}^{\mathrm{AS}}$, $\mathcal{H}^{\mathrm{AS}}$ and $\mathcal{H}_v$ are zero unless the conditions described in the following are satisfied:

$$\begin{aligned}&\mathcal{H}_{\mathrm{ST}}^{\mathrm{AS}}=1 \qquad \text{when } \dot{\overline{|\sigma_{\mathrm{ST}}|}}>0\\ &\quad\text{and } \sigma_{s,\mathrm{ST}}^{\mathrm{AS}}\leqslant|\sigma_{\mathrm{ST}}|\leqslant\sigma_{f,\mathrm{ST}}^{\mathrm{AS}}\\ &\mathcal{H}^{\mathrm{AS}}=1 \qquad \text{when } \dot{\overline{|\sigma|}}>0\\ &\quad\text{and } \sigma_s^{\mathrm{AS}}\leqslant|\sigma|\leqslant\sigma_f^{\mathrm{AS}}\\ &\mathcal{H}_v=1 \qquad \text{when } |\sigma|>|\sigma_{\mathrm{ST}}|\end{aligned}\tag{4}$$

where $\sigma_{s,\mathrm{ST}}^{\mathrm{AS}}$, σ_s^{AS}, $\sigma_{f,\mathrm{ST}}^{\mathrm{AS}}$ and σ_f^{AS} are material properties representing, respectively, the stress level at which the static and dynamic forward transformation starts and finishes. Finally, $\pi_{\mathrm{ST}}^{\mathrm{AS}}$, π^{AS}, $\beta_{\mathrm{ST}}^{\mathrm{AS}}$ and β^{AS} are material constants which govern, respectively, the speed of the static and dynamic phase transition evolution.

Conversion of martensite into austenite

$$\text{Linear}\begin{cases}\dot{\xi}_{\mathrm{ST}}=\xi_{\mathrm{ST}}\dfrac{\dot{\overline{|\sigma_{\mathrm{ST}}|}}}{|\sigma_{\mathrm{ST}}|-\sigma_{f,\mathrm{ST}}^{\mathrm{SA}}}\mathcal{H}_{\mathrm{ST}}^{\mathrm{SA}}\\ \dot{\xi}=\xi\dfrac{\dot{\overline{|\sigma|}}}{|\sigma|-\sigma_f^{\mathrm{SA}}}\mathcal{H}^{\mathrm{SA}}-\dfrac{\xi-\xi_{\mathrm{ST}}}{\tau}\,\mathcal{H}_v\end{cases}\tag{5}$$

$$\text{Power}\begin{cases}\dot{\xi}_{\mathrm{ST}}=\pi_{\mathrm{ST}}^{\mathrm{SA}}\xi_{\mathrm{ST}}\dfrac{\dot{\overline{|\sigma_{\mathrm{ST}}|}}}{|\sigma_{\mathrm{ST}}|-\sigma_{f,\mathrm{ST}}^{\mathrm{SA}}}\mathcal{H}_{\mathrm{ST}}^{\mathrm{SA}}\\ \dot{\xi}=\pi^{\mathrm{SA}}\xi\dfrac{\dot{\overline{|\sigma|}}}{|\sigma|-\sigma_f^{\mathrm{SA}}}\mathcal{H}^{\mathrm{SA}}-\dfrac{\xi-\xi_{\mathrm{ST}}}{\tau}\mathcal{H}_v\end{cases}\tag{6}$$

$$\text{Exponential}\begin{cases}\dot{\xi}_{\mathrm{ST}}=\beta_{\mathrm{ST}}^{\mathrm{SA}}\xi_{\mathrm{ST}}\dfrac{\dot{\overline{|\sigma_{\mathrm{ST}}|}}}{(|\sigma_{\mathrm{ST}}|-\sigma_{f,\mathrm{ST}}^{\mathrm{SA}})^2}\mathcal{H}_{\mathrm{ST}}^{\mathrm{SA}}\\ \dot{\xi}=\beta^{\mathrm{SA}}\xi\dfrac{\dot{\overline{|\sigma|}}}{(|\sigma|-\sigma_f^{\mathrm{SA}})^2}\mathcal{H}^{\mathrm{SA}}\\ \quad-\dfrac{\xi-\xi_{\mathrm{ST}}}{\tau}\mathcal{H}_v\end{cases}\tag{7}$$

where $\mathcal{H}_v$ is defined as above while $\mathcal{H}_{\mathrm{ST}}^{\mathrm{SA}}$ and $\mathcal{H}^{\mathrm{SA}}$ are zero unless the conditions described in the following are satisfied:

$$\begin{aligned}&\mathcal{H}_{\mathrm{ST}}^{\mathrm{SA}}=1 \qquad \text{when } \dot{\overline{|\sigma_{\mathrm{ST}}|}}<0\\ &\quad\text{and } \sigma_{f,\mathrm{ST}}^{\mathrm{SA}}\leqslant|\sigma_{\mathrm{ST}}|\leqslant\sigma_{s,\mathrm{ST}}^{\mathrm{SA}}\\ &\mathcal{H}^{\mathrm{SA}}=1 \qquad \text{when } \dot{\overline{|\sigma|}}<0 \quad\text{and}\quad \sigma_f^{\mathrm{SA}}\leqslant|\sigma|\leqslant\sigma_s^{\mathrm{SA}}\end{aligned}\tag{8}$$

where $\sigma_{s,\mathrm{ST}}^{\mathrm{SA}}$, σ_s^{SA}, $\sigma_{f,\mathrm{ST}}^{\mathrm{SA}}$ and σ_f^{SA} are material properties representing, respectively, the stress level at which the static and dynamic reverse transformation starts and finishes. Finally, $\pi_{\mathrm{ST}}^{\mathrm{SA}}$, π^{SA}, $\beta_{\mathrm{ST}}^{\mathrm{SA}}$ and β^{SA} are material constants which govern, respectively, the speed of the static and dynamic phase transition evolution.

We also note that it is possible to condense all the presented kinetic rules in a more general format:

$$A\to S\begin{cases}\dot{\xi}_{\mathrm{ST}}=\alpha_{\mathrm{ST}}^{\mathrm{AS}}(1-\xi_{\mathrm{ST}})\dfrac{\dot{\overline{|\sigma_{\mathrm{ST}}|}}}{(|\sigma_{\mathrm{ST}}|-\sigma_{f,\mathrm{ST}}^{\mathrm{AS}})^{\gamma_{\mathrm{ST}}^{\mathrm{AS}}}}\mathcal{H}_{\mathrm{ST}}^{\mathrm{AS}}\\ \dot{\xi}=\alpha^{\mathrm{AS}}(1-\xi)\dfrac{\dot{\overline{|\sigma|}}}{(|\sigma|-\sigma_f^{\mathrm{AS}})^{\gamma^{\mathrm{AS}}}}\mathcal{H}^{\mathrm{AS}}\\ \quad-\dfrac{\xi-\xi_{\mathrm{ST}}}{\tau}\mathcal{H}_v\end{cases}\tag{9}$$

$$S\to A\begin{cases}\dot{\xi}_{\mathrm{ST}}=\alpha_{\mathrm{ST}}^{\mathrm{SA}}\xi_{\mathrm{ST}}\dfrac{\dot{\overline{|\sigma_{\mathrm{ST}}|}}}{(|\sigma_{\mathrm{ST}}|-\sigma_{f,\mathrm{ST}}^{\mathrm{SA}})^{\gamma_{\mathrm{ST}}^{\mathrm{SA}}}}\mathcal{H}_{\mathrm{ST}}^{\mathrm{SA}}\\ \dot{\xi}=\alpha^{\mathrm{SA}}\xi\dfrac{\dot{\overline{|\sigma|}}}{(|\sigma|-\sigma_f^{\mathrm{SA}})^{\gamma^{\mathrm{SA}}}}\mathcal{H}^{\mathrm{SA}}\\ \quad-\dfrac{\xi-\xi_{\mathrm{ST}}}{\tau}\mathcal{H}_v\end{cases}\tag{10}$$

where $\alpha_{\mathrm{ST}}^{\mathrm{AS}}$, α^{AS}, $\alpha_{\mathrm{ST}}^{\mathrm{SA}}$ and α^{SA} are material constants and where $\gamma_{\mathrm{ST}}^{\mathrm{AS}}$, γ^{AS}, $\gamma_{\mathrm{ST}}^{\mathrm{SA}}$ and γ^{SA} are parameters that may only assume the integer values 1 or 2 depending on the selected type of kinetic rule (i.e. in particular, 1 if we adopt linear or power kinetic rules, 2 if we adopt exponential kinetic rules).

3.5. Evolution of elastic modulus

Experimental tests show large differences between the elastic properties of austenite and martensite [1, 7, 8, 10]. To model this aspect, we introduce a *static elastic modulus* and a *dynamic elastic modulus*, respectively denoted as E_{ST} and E, functions of the corresponding martensite fractions:

$$E_{\mathrm{ST}}=E_{\mathrm{ST}}(\xi_{\mathrm{ST}}) \tag{11a}$$

$$E=E(\xi). \tag{11b}$$

Valid expressions for the above quantities can be obtained by regarding the SMA as a composite material made of a volume fraction of martensite and a volume fraction of austenite. Next, the overall elastic properties can be recovered through the homogenization theory.

Addressing the reader to more specific works regarding such a topic, for the specific problem under investigation (i.e. uniaxial state of stress in wires and bars subjected to cyclic loadings), we follow references [2] and [13] and adopt a Reuss scheme. In particular, knowing the elastic modulus of the pure austenite, E_A, and the pure martensite, E_S, the equivalent moduli are expressed as:

$$E_{\mathrm{ST}}=\frac{E_AE_S}{E_S+(E_A-E_S)\xi_{\mathrm{ST}}} \tag{12a}$$

$$E=\frac{E_AE_S}{E_S+(E_A-E_S)\xi}. \tag{12b}$$

However, it should be noted that the previous expressions provide lower bounds for the overall elastic moduli, since the cross sections of the SMA elements under consideration are large if compared to the length scale involved in the homogenization of austenite and martensite. More precisely, the realistic values would lie between these and the ones given by the Voigt scheme, which instead provides upper bounds [1].

3.6. Stress–strain relationships

Consistently with the previous considerations, we introduce two different inelastic strains, the *static inelastic strain*, $\epsilon^{\text{in}}_{\text{ST}}$, and the *dynamic inelastic strain*, ϵ^{in}, the former representing the inelastic strain that would be obtained in the case of static loading conditions. These strains are related to the corresponding martensite fractions as follows:

$$\epsilon^{\text{in}}_{\text{ST}} = \epsilon_L \xi_{\text{ST}} \text{sgn}(\sigma_{\text{ST}}) \tag{13a}$$

$$\epsilon^{\text{in}} = \epsilon_L \xi \,\text{sgn}(\sigma) \tag{13b}$$

where ϵ_L is the maximum residual strain (i.e. a measure of the maximum deformation obtainable aligning all the single-variant martensites in one direction), sgn(·) is the sign function and σ_{ST} and σ are, respectively, the static and the dynamic stress.

Recalling that we are limiting the discussion to a small deformation regime, for the *total strain*, ϵ, we may introduce two additive decompositions:

$$\epsilon = \epsilon^{\text{el}}_{\text{ST}} + \epsilon^{\text{in}}_{\text{ST}} \tag{14a}$$

$$\epsilon = \epsilon^{\text{el}} + \epsilon^{\text{in}} \tag{14b}$$

where $\epsilon^{\text{el}}_{\text{ST}}$ represents the *static elastic strain* and ϵ^{el} the *dynamic elastic strain*. Finally, by assuming the previous stress states to be linearly related to the corresponding elastic strains, we can write:

$$\begin{aligned}\sigma_{\text{ST}} &= E_{\text{ST}}\epsilon^{\text{el}}_{\text{ST}} = E_{\text{ST}}(\epsilon - \epsilon^{\text{in}}_{\text{ST}}) \\ &= E_{\text{ST}}\left[\epsilon - \epsilon_L \xi_{\text{ST}} \text{sgn}(\sigma_{\text{ST}})\right]\end{aligned} \tag{15a}$$

$$\sigma = E\epsilon^{\text{el}} = E(\epsilon - \epsilon^{\text{in}}) = E\left[\epsilon - \epsilon_L \xi \,\text{sgn}(\sigma)\right]. \tag{15b}$$

4. Time-discrete model and solution algorithms

During the development of the time-continuous model we assumed the stress as control variable. However, for the development of the time-discrete model we assume the strain as control variable. This choice is consistent with the fact that, from the integration scheme point of view, the time-discrete problem is interpreted as strain-driven. Accordingly, we consider two instants, t_n and $t_{n+1} > t_n$, such that t_{n+1} is the first time value of interest after t_n. Next, knowing the strain at time t_{n+1} and the solution at time t_n, we should compute the new solution at time t_{n+1}.

To minimize the appearance of subscripts, we introduce the convention:

$$a_n = a(t_n), \qquad a = a(t_{n+1})$$

where a is a generic quantity. Therefore, the subscript n indicates a quantity evaluated at time t_n, while no subscript indicates a quantity evaluated at time t_{n+1}.

We also observe that, by manipulating equations (15*a*) and (15*b*), it would be possible to conclude that $\text{sgn}(\sigma_{\text{ST}}) = \text{sgn}(\sigma) = \text{sgn}(\epsilon)$. This consideration is of interest, since in a time-discrete setting ϵ is assumed to be known at any instant.

4.1. Time-discrete model

We first need to introduce the static and dynamic martensite fraction increments, λ_{ST} and λ, respectively defined as:

$$\xi_{\text{ST}} = \xi_{ST,n} + \lambda_{\text{ST}} \qquad \text{or} \qquad \lambda_{\text{ST}} = \int_{t_n}^{t_{n+1}} \dot{\xi}_{\text{ST}}\, \text{d}t \tag{16a}$$

$$\xi = \xi_n + \lambda \qquad \text{or} \qquad \lambda = \int_{t_n}^{t_{n+1}} \dot{\xi}\, \text{d}t. \tag{16b}$$

We then use a backward-Euler scheme to integrate the kinetic rules presented in section 3.4. In particular, written in residual form and after clearing the fractions, the time-discrete evolutionary equations assume the following expressions.

Conversion of austenite into martensite

$$\text{Linear} \begin{cases} \mathcal{R}^{\text{AS}}_{\text{ST}} = \lambda_{\text{ST}}(|\sigma_{\text{ST}}| - \sigma^{\text{AS}}_{f,\text{ST}}) \\ \quad + (1-\xi_{\text{ST}})(|\sigma_{\text{ST}}| - |\sigma_{\text{ST},n}|)\mathcal{H}^{\text{AS}}_{\text{ST}} = 0 \\ \mathcal{R}^{\text{AS}} = \lambda(|\sigma| - \sigma^{\text{AS}}_f) \\ \quad + (1-\xi)(|\sigma| - |\sigma_n|)\mathcal{H}^{\text{AS}} \\ \quad + \dfrac{\Delta t}{\tau}(\xi - \xi_{\text{ST}})(|\sigma| - \sigma^{\text{AS}}_f)\mathcal{H}_v = 0 \end{cases} \tag{17}$$

$$\text{Power} \begin{cases} \mathcal{R}^{\text{AS}}_{\text{ST}} = \lambda_{\text{ST}}(|\sigma_{\text{ST}}| - \sigma^{\text{AS}}_{f,\text{ST}}) \\ \quad + \pi^{\text{AS}}_{\text{ST}}(1-\xi_{\text{ST}})(|\sigma_{\text{ST}}| - |\sigma_{\text{ST},n}|)\mathcal{H}^{\text{AS}}_{\text{ST}} = 0 \\ \mathcal{R}^{\text{AS}} = \lambda(|\sigma| - \sigma^{\text{AS}}_f) \\ \quad + \pi^{\text{AS}}(1-\xi)(|\sigma| - |\sigma_n|)\mathcal{H}^{\text{AS}} \\ \quad + \dfrac{\Delta t}{\tau}(\xi - \xi_{\text{ST}})(|\sigma| - \sigma^{\text{AS}}_f)\mathcal{H}_v = 0 \end{cases} \tag{18}$$

$$\text{Exponential} \begin{cases} \mathcal{R}^{\text{AS}}_{\text{ST}} = \lambda_{\text{ST}}(|\sigma_{\text{ST}}| - \sigma^{\text{AS}}_{f,\text{ST}})^2 \\ \quad - \beta^{\text{AS}}_{\text{ST}}(1-\xi_{\text{ST}})(|\sigma_{\text{ST}}| - |\sigma_{\text{ST},n}|)\mathcal{H}^{\text{AS}}_{\text{ST}} = 0 \\ \mathcal{R}^{\text{AS}} = \lambda(|\sigma| - \sigma^{\text{AS}}_f)^2 \\ \quad - \beta^{\text{AS}}(1-\xi)(|\sigma| - |\sigma_n|)\mathcal{H}^{\text{AS}} \\ \quad + \dfrac{\Delta t}{\tau}(\xi - \xi_{\text{ST}})(|\sigma| - \sigma^{\text{AS}}_f)^2\mathcal{H}_v = 0. \end{cases} \tag{19}$$

Conversion of martensite into austenite

$$\text{Linear} \begin{cases} \mathcal{R}^{\text{SA}}_{\text{ST}} = \lambda_{\text{ST}}(|\sigma_{\text{ST}}| - \sigma^{\text{SA}}_{f,\text{ST}}) \\ \quad - \xi_{\text{ST}}(|\sigma_{\text{ST}}| - |\sigma_{\text{ST},n}|)\mathcal{H}^{\text{SA}}_{\text{ST}} = 0 \\ \mathcal{R}^{\text{SA}} = \lambda(|\sigma| - \sigma^{\text{SA}}_f) - \xi(|\sigma| - |\sigma_n|)\mathcal{H}^{\text{SA}} \\ \quad + \dfrac{\Delta t}{\tau}(\xi - \xi_{\text{ST}})(|\sigma| - \sigma^{\text{SA}}_f)\mathcal{H}_v = 0 \end{cases} \tag{20}$$

$$\text{Power} \begin{cases} \mathcal{R}^{\text{SA}}_{\text{ST}} = \lambda_{\text{ST}}(|\sigma_{\text{ST}}| - \sigma^{\text{SA}}_{f,\text{ST}}) \\ \quad - \pi^{\text{SA}}_{\text{ST}}\xi_{\text{ST}}(|\sigma_{\text{ST}}| - |\sigma_{\text{ST},n}|)\mathcal{H}^{\text{SA}}_{\text{ST}} = 0 \\ \mathcal{R}^{\text{SA}} = \lambda(|\sigma| - \sigma^{\text{SA}}_f) - \pi^{\text{SA}}\xi(|\sigma| - |\sigma_n|)\mathcal{H}^{\text{SA}} \\ \quad + \dfrac{\Delta t}{\tau}(\xi - \xi_{\text{ST}})(|\sigma| - \sigma^{\text{SA}}_f)\mathcal{H}_v = 0 \end{cases} \tag{21}$$

Table 1. Overall strain-driven solution algorithm.

1. Detect loading or unloading
   If $|\epsilon - \epsilon_n| > 0 \Rightarrow$ loading
   If $|\epsilon - \epsilon_n| < 0 \Rightarrow$ unloading
2. Check phase transformation
   if loading then
   check $A \rightarrow S$ phase transformation (table 2)
   else if unloading then
   check $S \rightarrow A$ phase transformation (table 3)
   end if
3. Compute stress

$$\text{Exponential} \begin{cases} \mathcal{R}^{\text{SA}}_{\text{ST}} = \lambda_{\text{ST}}(|\sigma_{\text{ST}}| - \sigma^{\text{SA}}_{f,\text{ST}})^2 \\ \quad - \beta^{\text{SA}}_{\text{ST}} \xi_{\text{ST}}(|\sigma_{\text{ST}}| - |\sigma_{\text{ST},n}|)\mathcal{H}^{\text{SA}}_{\text{ST}} = 0 \\ \mathcal{R}^{\text{SA}} = \lambda(|\sigma| - \sigma^{\text{SA}}_f)^2 \\ \quad - \beta^{\text{SA}} \xi(|\sigma| - |\sigma_n|)\mathcal{H}^{\text{SA}} \\ \quad + \dfrac{\Delta t}{\tau}(\xi - \xi_{\text{ST}})(|\sigma| - \sigma^{\text{SA}}_f)^2 \mathcal{H}_v = 0. \end{cases} \tag{22}$$

4.2. Solution algorithms

To solve the time-discrete evolutionary equations presented in the previous section, we can either adopt an interactive strategy or consider a closed-form solution approach, as briefly discussed in the following.

(i) *Solution by iterative strategy.* As an iterative strategy, we select the Newton–Raphson scheme. To guarantee the method quadratic convergence, the derivatives of the evolutionary equations written in residual form are required in order to obtain the tangent modulus consistent with the time-discrete model. For brevity, we do not include them here but their computation is straightforward.

(ii) *Solution in closed-form.* Limiting the discussion to the computation of the dynamic martensite fraction, substitution of equation (15*b*) into equations (17)–(22), returns expressions of the type:

$$\begin{aligned} C_2\xi^2 + C_1\xi + C_0 &= 0 \\ C_3\xi^3 + C_2\xi^2 + C_1\xi + C_0 &= 0 \end{aligned} \tag{23}$$

whose roots can be easily found in closed-form. In particular, we obtain a quadratic expression when considering both linear and power rules and a cubic expression when considering the exponential rules. The coefficients C_0, C_1, C_2 and C_3 are not reported for brevity. Moreover, due to their complexity, it does not seem reasonable to perform a discussion of the equation roots. As a consequence, the admissible root is chosen as the one bounded between 0 (phase transformation not started yet) and 1 (complete phase transformation).

In view of the computer implementation of the model, in table 1 we summarize the main steps concerning the overall strain-driven solution algorithm and in tables 2 and 3 we provide the solution schemes related, for brevity, only to the dynamic forward and reverse phase transformation.

Table 2. Solution scheme for the dynamic $A \rightarrow S$ phase transformation.

If $|\epsilon - \epsilon_n| > 0$ then $\Rightarrow$ loading

$$\epsilon^{AS}_s = \text{sgn}(\epsilon)\,\frac{\sigma^{AS}_s}{E_n} + \text{sgn}(\epsilon)\,\xi_n\,\epsilon_L$$

$$\epsilon^{AS}_f = \text{sgn}(\epsilon)\,\frac{\sigma^{AS}_f}{E_n} + \text{sgn}(\epsilon)\,\epsilon_L$$

if $|\epsilon - \epsilon_n| \leq \epsilon^{AS}_s$

$$\xi = \xi_n$$
$$E = E_n$$

else if $|\epsilon - \epsilon_n| > \epsilon^{AS}_s$ and $|\epsilon - \epsilon_n| < \epsilon^{AS}_f$

Solve $\mathcal{R}^{AS} = 0$ { Iterative strategy / Closed-form solution

$$E = \frac{E_A\,E_S}{E_S + \xi\,(E_A - E_S)}$$

else

$$\xi = 1$$
$$E = E_S$$

end

end

5. Numerical investigations

We now want to understand the role of the coefficients which appear in the kinetic rules, distinguishing parameters governing the evolution of the static martensite fraction from parameters governing the evolution of the dynamic martensite fraction. Accordingly, we investigate the ability of the model to simulate the typical superelastic SMA stress–strain response by considering three numerical tests.

- *Test 1.* Strain-controlled loading–unloading cycle performed in static conditions up to a 7% strain. The aim of this test is to simulate a number of superelastic responses by changing the values of the speed parameters (i.e. π_{ST}s and β_{ST}s).
- *Test 2.* Strain-controlled loading–unloading cycle performed at different speeds (corresponding to slow, moderate and fast loading conditions) up to a 7% strain. In particular, this test is obtained by applying the loading–unloading pattern in 10^3, 1 and 10^{-3} s, respectively. The aim of this test is to simulate the rate-dependent superelastic response exhibited by the proposed model.
- *Test 3.* Strain-controlled loading–unloading cycle performed at different speeds up to a 7% strain. First, a loading pattern is applied by means of two ramps performed in 10^{-3} s each and separated by a time interval of 10^3 s of constant strain, then an unloading pattern performed in 10^{-3} s follows. The aim of this test is to simulate the relaxation effect exhibited by the proposed model.

Nonetheless, the capability of the model to describe the material behaviour also for more complex loading histories

Table 3. Solution scheme for the dynamic $S \rightarrow A$ phase transformation.

If $|\epsilon - \epsilon_n| < 0$ then $\Rightarrow$ unloading

$$\epsilon_s^{SA} = \text{sgn}(\epsilon)\,\frac{\sigma_s^{SA}}{E_n} + \text{sgn}(\epsilon)\,\xi_n\,\epsilon_L$$

$$\epsilon_f^{SA} = \text{sgn}(\epsilon)\,\frac{\sigma_f^{SA}}{E_n}$$

if $|\epsilon - \epsilon_n| \geq \epsilon_s^{SA}$

$$\xi = \xi_n$$

$$E = E_n$$

else if $|\epsilon - \epsilon_n| < \epsilon_s^{SA}$ and $|\epsilon - \epsilon_n| > \epsilon_f^{SA}$

Solve $\mathcal{R}^{SA} = 0$ { Iterative strategy / Closed-form solution

$$E = \frac{E_A\,E_S}{E_S + \xi\,(E_A - E_S)}$$

else

$$\xi = 0$$

$$E = E_A$$

end

end

(such as partial and complete tension-compression loading–unloading patterns with the description of inner hysteresis loops) has been numerically tested but not reported here for brevity.

For the numerical simulations, we consider the following material properties:

$$E_A = 40\,000 \text{ MPa} \qquad E_S = 20\,000 \text{ MPa}$$

$$\epsilon_L = 5\% \qquad \tau = 0.5 \text{ s}$$

$$\sigma_{s,\text{ST}}^{\text{AS}} = 200 \text{ MPa} \qquad \sigma_{f,\text{ST}}^{\text{AS}} = 300 \text{ MPa}$$

$$\sigma_{s,\text{ST}}^{\text{SA}} = 200 \text{ MPa} \qquad \sigma_{f,\text{ST}}^{\text{SA}} = 100 \text{ MPa}$$

$$\sigma_s^{\text{AS}} = 200 \text{ MPa} \qquad \sigma_f^{\text{AS}} = 1000 \text{ MPa}$$

$$\sigma_s^{\text{SA}} = 800 \text{ MPa} \qquad \sigma_f^{\text{SA}} = 100 \text{ MPa}$$

where it is important to observe that we choose $\sigma_{s,\text{ST}}^{\text{AS}} = \sigma_s^{\text{AS}}$ and $\sigma_{f,\text{ST}}^{\text{SA}} = \sigma_f^{\text{SA}}$ (i.e. the stress level at which the austenite-to-martensite phase transformation starts and the stress level at which the martensite-to-austenite phase transformation finishes is the same for both the static and the dynamic case).

Moreover, for most of the numerical simulations performed in the present section and unless explicitly stated, we adopt constant values for the static and the dynamic speed parameters (i.e. we set $\pi_{\text{ST}}^{\text{AS}} = \pi^{\text{AS}} = \pi_{\text{ST}}^{\text{SA}} = \pi^{\text{SA}} = \pi$ for the power rules and $\beta_{\text{ST}}^{\text{AS}} = \beta^{\text{AS}} = \beta_{\text{ST}}^{\text{SA}} = \beta^{\text{SA}} = \beta$ for the exponential rules). This choice is done to reduce the number of results to be reported but, as is clear from them, it is quite limiting and, consequently, it will be removed later.

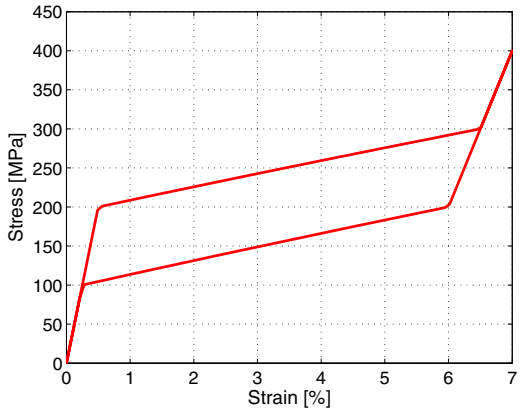

Figure 1. Linear kinetic rules: evolution of the stress–strain relationship for static loading conditions.

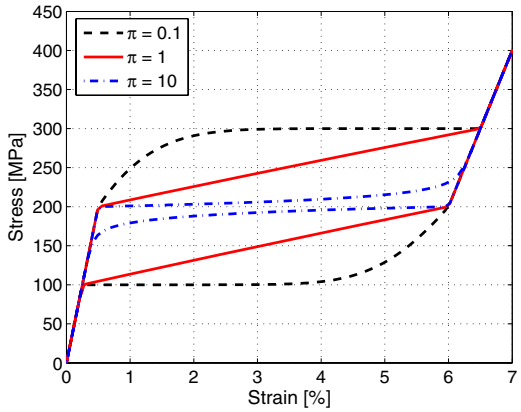

Figure 2. Power kinetic rules: evolution of the stress–strain relationship for static loading conditions.

5.1. Model response

The results from test 1 (static loading conditions) are reported in figures 1–3 in terms of stress–strain relationships and for the three kinetic rules. From the result examination, we may draw the following conclusions.

- The linear rules (figure 1) describe the superelastic behaviour by linearly connecting the corresponding start and finish transformation stress levels, therefore without reproducing the typical smooth behaviour displayed by most SMAs.
- The power rules (figure 2) show different behaviours according to the values of π parameters. In particular, for π below or above 1 the curve representing the phase transition evolution changes convexity. In fact, the smaller the π values, the faster the model response to reach the final transformation stress levels, while the higher the π values, the slower the model response to reach the final transformation stress levels. Finally, also from a numerical point of view, the power rules reproduce a linear kinetics upon setting $\pi = 1$.
- The exponential rules (figure 3) show different behaviours according to the values of β parameters. In particular, by choosing β in the positive range it is possible to control the

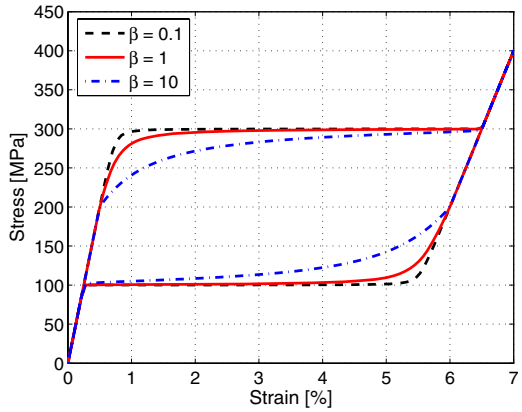

Figure 3. Exponential kinetic rules: evolution of the stress–strain relationship for static loading conditions.

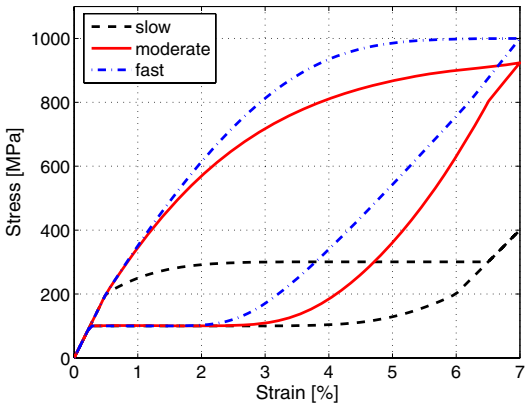

Figure 5. Power kinetic rules: evolution of the stress–strain relationship for slow, moderate and fast loading conditions ($\pi = 0.1$).

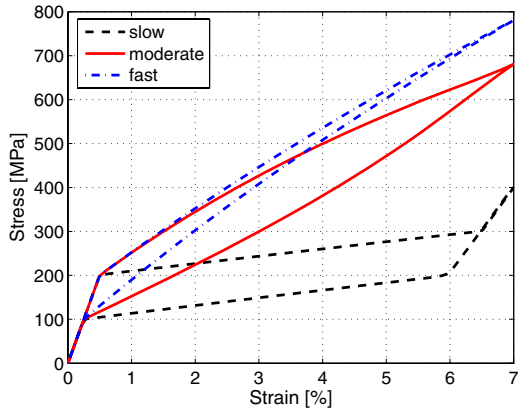

Figure 4. Linear kinetic rules: evolution of the stress–strain relationship for slow, moderate and fast loading conditions.

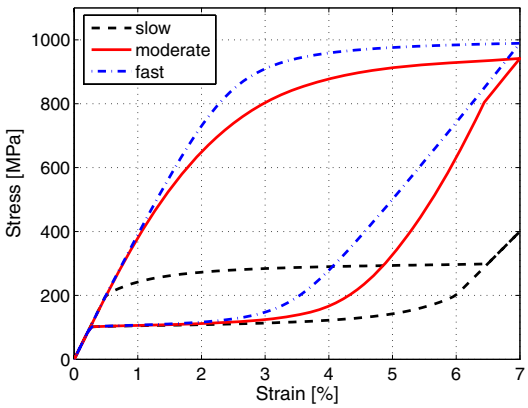

Figure 6. Exponential kinetic rules: evolution of the stress–strain relationship for slow, moderate and fast loading conditions ($\beta = 10$).

speed of the phase transition saturation without, however, having the possibility of changing the convexity of the curve as for the power rules (figure 2).

The results from test 2 (dynamic loading conditions) are reported in figures 4–6 in terms of stress–strain relationships and for the three kinetic rules. From the result examination, we may draw the following conclusions.

- All rules are able to reproduce the experimentally observed [7, 8, 11] increase of the stress level at which the forward and reverse transformation takes place as the loading frequency increases.
- The linear rules (figure 4) are able to reproduce the experimentally observed [7, 8, 11] hysteresis size reduction with the increase of the loading rate. Furthermore, the higher the frequency, the faster the response to approach the final phase transformation stress value.
- The power rules (figure 5) do not seem to reproduce the hysteresis size reduction, meaning that there is an overestimation of the dissipated energy. However, this effect is also due to the arbitrary choice of setting $\pi_{\mathrm{ST}}^{\mathrm{AS}} = \pi^{\mathrm{AS}} = \pi_{\mathrm{ST}}^{\mathrm{SA}} = \pi^{\mathrm{SA}} = \pi$. In fact, by choosing different values for the static and the dynamic speed factors it would instead be possible to model a significant hysteresis size reduction.
- Also the exponential rules (figure 6) do not seem to reproduce the hysteresis size reduction, meaning that there is an overestimation of the dissipated energy. Again, this effect is also due to the arbitrary choice of setting $\beta_{\mathrm{ST}}^{\mathrm{AS}} = \beta^{\mathrm{AS}} = \beta_{\mathrm{ST}}^{\mathrm{SA}} = \beta^{\mathrm{SA}} = \beta$. As in the previous case, by choosing different values for the static and the dynamic speed factors it would still be possible to predict a significant size reduction of the hysteretic loop.

The results from test 3 (simulation of the relaxation effect) are reported in figures 7–9 in terms of stress–strain relationships and for the three kinetic rules. From the result examination, we may draw the following conclusions.

- In figures 7–9, we observe the relaxation effect exhibited by the proposed model. After a first ramp up to a 4% strain performed in fast loading conditions in which the stress level keeps increasing, the actual stress level drops to the same value of the corresponding static one because of the effect simulated by the viscous term included in the kinetic rules. This behaviour is due to the presence of a constant strain level which follows the first loading pattern. Then,

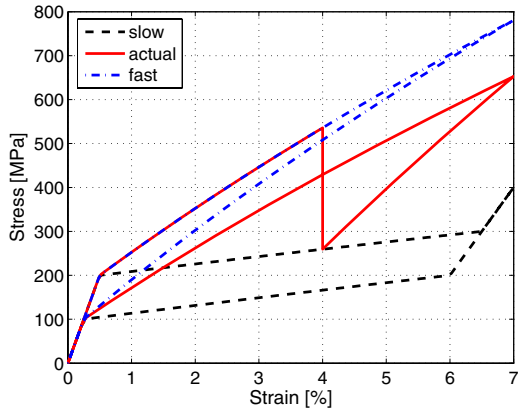

Figure 7. Linear kinetic rules: simulation of the relaxation effect.

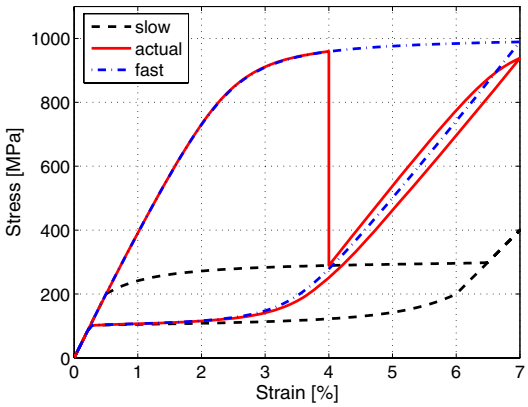

Figure 9. Exponential kinetic rules: simulation of the relaxation effect ($\beta = 10$).

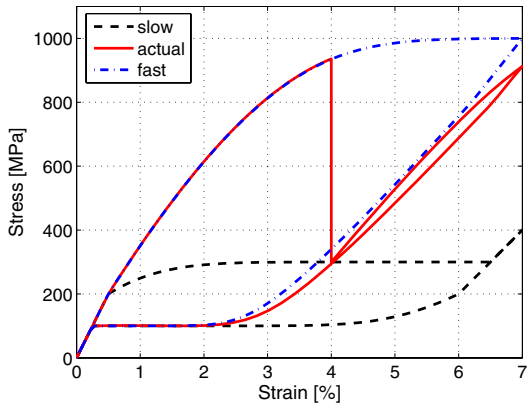

Figure 8. Power kinetic rules: simulation of the relaxation effect ($\pi = 0.1$).

another ramp performed at the same speed as the first one is applied and the stress value tends to reach that at which the dynamic forward transformation finishes. Finally, an unloading ramp performed in fast loading conditions completes the loading–unloading history.

- As noticed in the second numerical test (dynamic loading conditions), the speed parameters play a fundamental role in describing the hysteretic loop. Again, by distinguishing speed parameters related to the static phase transformations from speed parameters related to the dynamic phase transformations, it would still be possible to simulate a number of stress–strain relationships.

Furthermore, in agreement with [1], numerical tests not included have showed that the model response is always contained between the very fast and the very slow responses, which are the limiting behaviours.

6. Experimental investigation and model fitting ability

The goal is now to validate the ability of the model to reproduce the rate-dependent superelastic behaviour of SMA elements. We do this by comparing the numerical response with available experimental data related to superelastic NiTi SMA wires and bars of different size and chemical composition, tested at frequency levels which are typical for structural applications in earthquake engineering [7, 8, 10].

We focus attention on three sets of materials, as discussed in the following.

- *Set 1.* The material is a commercial superelastic NiTi straight wire with circular cross section of diameter 0.76 mm provided by Memry Corp. (Menlo Park, USA). The testing frequencies were 0.001 Hz (static) and 0.1 Hz (dynamic).
- *Set 2.* The material is a commercial superelastic NiTi straight wire with circular cross section of diameter 1.00 mm provided by CNR-IENI (Lecco, Italy). The testing frequencies were 0.001 Hz (static) and 1 Hz (dynamic).
- *Set 3.* The material is a commercial superelastic NiTi bar with circular cross section of diameter 7.1 mm provided by Special Metals Corporation (New Hartford, USA). The testing frequencies were 0.025 Hz (static) and 1 Hz (dynamic).

The experimental data are obtained from uniaxial tests consisting of multiple strain-driven loading–unloading cycles performed on virgin material and at room temperature (≈20 °C). In particular, the loading protocol used for the first two sets consisted of increasing strain cycles of 1% to 6% by increments of 1% while the loading protocol used for the third set consisted of increasing strain cycles of 0.5%, 1.0% to 5% by increments of 1% followed by four cycles at 6%. For simplicity, and following the same comparison strategy presented in work [3], we only consider a single cycle up to a 6% strain. However, it should be remarked that additional experiments consisting, for instance, of more complex deformation time histories and corresponding comparisons with numerical results would give a much better feedback of the model fitting ability.

Tests relative to set 1 and set 2 were performed at the Parco Scientifico Tecnologico e delle Telecomunicazioni in Valle Scrivia (Tortona, Italy) by Fugazza [10], while tests relative to set 3 were performed by DesRoches *et al* [7] at the Georgia Institute of Technology (Atlanta, USA). Both experimental investigations were aimed at studying the cyclic properties of superelastic SMA elements for seismic applications.

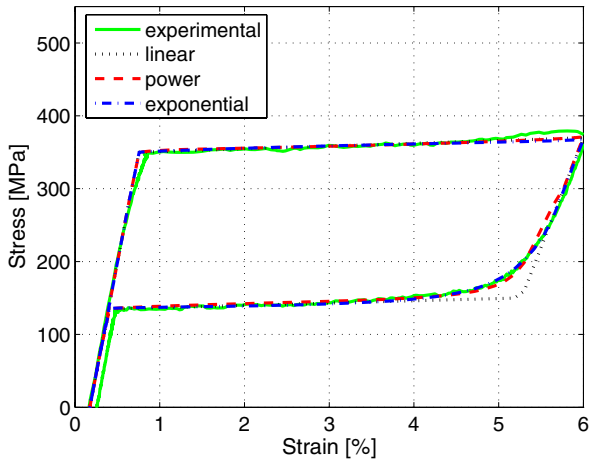

Figure 10. Static loading conditions: experimental data (set 1) versus numerical results.

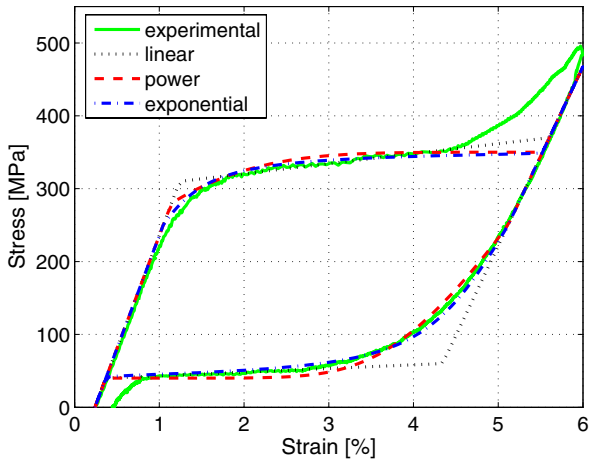

Figure 12. Static loading conditions: experimental data (set 2) versus numerical results.

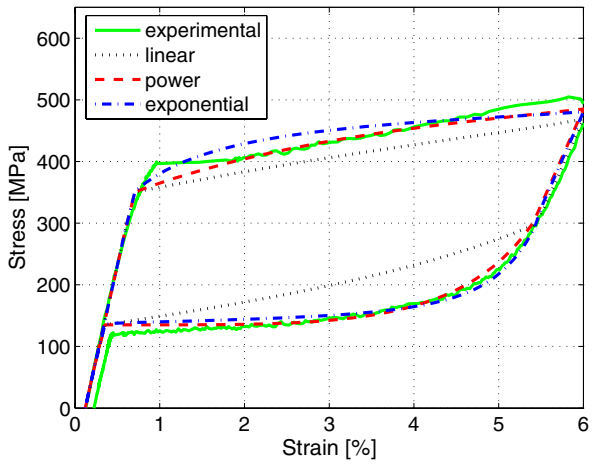

Figure 11. Dynamic loading conditions: experimental data (set 1) versus numerical results.

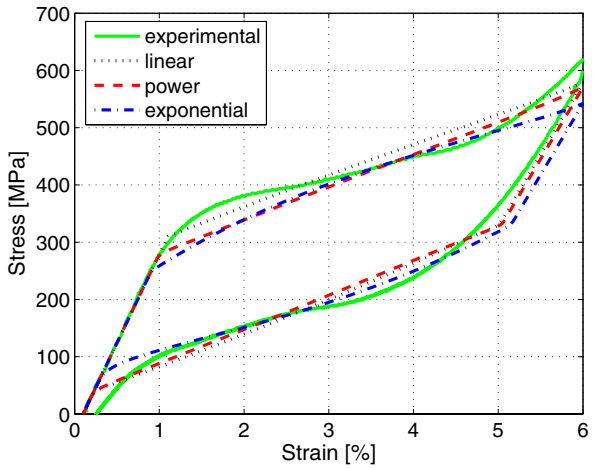

Figure 13. Dynamic loading conditions: experimental data (set 2) versus numerical results.

To properly choose the model parameters (table 4) related to each set of experimental data, we should sequentially perform the steps listed in the following. We also recall that *a priori* we set $\sigma^{\mathrm{AS}}_{s,\mathrm{ST}} = \sigma^{\mathrm{AS}}_{s}$ and $\sigma^{\mathrm{SA}}_{f,\mathrm{ST}} = \sigma^{\mathrm{SA}}_{f}$.

(i) Obtain E_A, E_S and ϵ_L from all experimental curves belonging to the same set.

(ii) Obtain $\sigma^{\mathrm{AS}}_{s,\mathrm{ST}}$, $\sigma^{\mathrm{AS}}_{f,\mathrm{ST}}$, $\sigma^{\mathrm{SA}}_{s,\mathrm{ST}}$ and $\sigma^{\mathrm{SA}}_{f,\mathrm{ST}}$ from the test performed at the lowest frequency (these data may vary according to the adopted kinetic rule).

(iii) Compute $\pi^{\mathrm{AS}}_{\mathrm{ST}}$ and $\pi^{\mathrm{SA}}_{\mathrm{ST}}$, when considering power rules, as well as $\beta^{\mathrm{AS}}_{\mathrm{ST}}$ and $\beta^{\mathrm{SA}}_{\mathrm{ST}}$, when considering exponential rules, from the test performed at the lowest frequency.

(iv) Compute π^{AS} and π^{SA} when considering power rules, β^{AS} and β^{SA} when considering exponential rules and obtain σ^{AS}_{f} and σ^{SA}_{s}, from the test performed at the highest frequency.

Figures 10–15 report the comparison between the experimental data and the model responses. From the result examination, we may draw the following conclusions.

- From the analysis of the static tests (figures 10, 12 and 14), we note a very good match between experiments and numerical results, especially when power and exponential rules are considered.
- From the analysis of the dynamic tests (figures 11, 13 and 15), we observe that the model performance strongly depends on the SMA material under investigation. In fact, for the first and third material the best fitting is obtained using both power and exponential rules (figures 11 and 15), while for the second material the best fitting is obtained when considering the linear rules (figure 13). Also, as experimental tests display [7, 8, 10], the hysteresis size reduction as well as the hardening of the material is always noticed for high strain rates.
- From the analysis of both static and dynamic tests (figures 12–15), we notice the excellent ability of the model to capture the maximum stress level attained at the end of the loading phase.

7. Conclusions

In this paper we presented a uniaxial rate-dependent viscous constitutive model capable of reproducing the superelastic

Table 4. Material properties (L = linear kinetic rules, P = power kinetic rules, E = exponential kinetic rules).

		Set 1			Set 2			Set 3		
		L	P	E	L	P	E	L	P	E
E_A	[MPa]	61 000	61 000	61 000	31 000	31 000	31 000	35 000	35 000	35 000
E_S	[MPa]	30 000	30 000	30 000	24 600	24 600	24 600	28 000	28 000	28 000
ϵ_L	[%]	4.80	4.80	4.80	4.10	4.10	4.10	4.25	4.25	4.25
τ	[s]	0.9	0.9	0.9	0.9	0.9	0.9	0.9	0.9	0.9
$\sigma^{\mathrm{AS}}_{s,\mathrm{ST}}$	[MPa]	350	350	350	310	280	250	320	340	340
$\sigma^{\mathrm{AS}}_{f,\mathrm{ST}}$	[MPa]	370	370	370	350	350	350	460	460	460
$\sigma^{\mathrm{SA}}_{s,\mathrm{ST}}$	[MPa]	150	150	250	60	250	250	260	400	400
$\sigma^{\mathrm{SA}}_{f,\mathrm{ST}}$	[MPa]	135	135	135	40	40	40	190	200	200
σ^{AS}_{f}	[MPa]	500	500	500	620	620	620	520	520	520
σ^{SA}_{s}	[MPa]	300	300	300	330	330	330	320	320	420
$\pi^{\mathrm{AS}}_{\mathrm{ST}}$	[—]	—	1.5	—	—	0.18	—	—	1	—
$\pi^{\mathrm{SA}}_{\mathrm{ST}}$	[—]	—	1.5	—	—	0.12	—	—	0.09	—
$\beta^{\mathrm{AS}}_{\mathrm{ST}}$	[—]	—	—	15	—	—	6	—	—	140
$\beta^{\mathrm{SA}}_{\mathrm{ST}}$	[—]	—	—	4	—	—	9.8	—	—	15
π^{AS}	[—]	—	0.5	—	—	1.1	—	—	1	—
π^{SA}	[—]	—	0.2	—	—	1.1	—	—	2	—
β^{AS}	[—]	—	—	25	—	—	240	—	—	50
β^{SA}	[—]	—	—	10	—	—	200	—	—	130

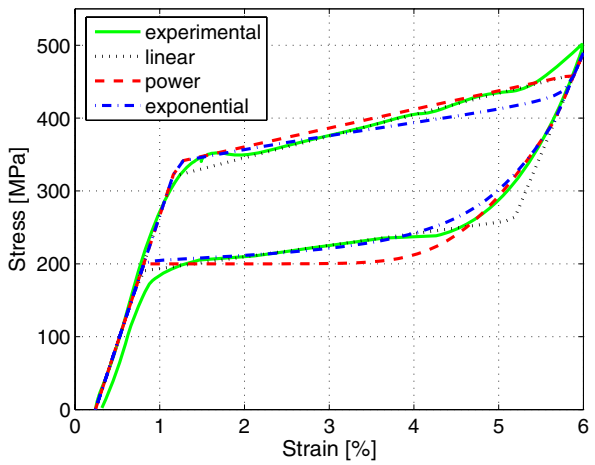

Figure 14. Static loading conditions: experimental data (set 3) versus numerical results.

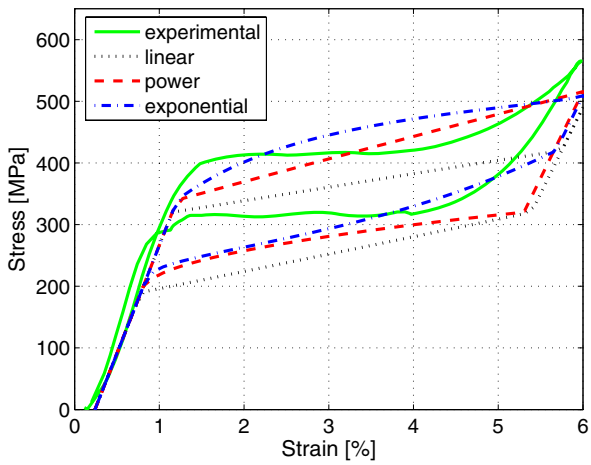

Figure 15. Dynamic loading conditions: experimental data (set 3) versus numerical results.

effect of SMAs and able to take into account the different elastic properties between austenite and martensite.

In the following, we summarize the most important findings of the research by briefly reviewing the general features of the model as well as by discussing the results obtained from the numerical tests and the comparisons with experimental data.

- The formulation of the model is based on two scalar internal variables, the static martensite fraction and the dynamic martensite fraction, for which three different types of evolutionary equations in rate form are proposed.
- The model requires a limited number of material parameters which may be obtained from standard uniaxial tests. They are the Young's modulus of austenite and martensite, the plateau length, the stress levels (in static and dynamic conditions) at which the forward and reverse transformation takes place and a measure of the transformation speed.
- By considering power and exponential kinetic rules, it is possible to simulate the smooth transition from the elastic regions to the phase transition regions, as experimental evidence displays.
- The ability of the model to simulate experimental data relative to uniaxial tests performed on SMA wires and bars in both static and dynamic loading conditions has also been assessed. Static tests have provided a very good comparison between experiments and numerical analyses, meanwhile dynamic tests were strongly affected by the

different rate-dependent responses (i.e. different stress–strain relationship exhibited by each SMA for the same loading frequency) of the considered SMA materials.

In conclusion, the advantages of the presented model are the simplicity, the possibility of implementing a robust solution algorithm and the ability to reproduce experimental data obtained from uniaxial tests performed on SMA elements at different frequency levels of excitation.

Acknowledgments

The second author of this paper would like to thank Ms Federica Onano of Parco Scientifico Tecnologico e delle Telecomunicazioni in Valle Scrivia (Tortona, Italy) and Dr Lorenza Petrini of Politecnico di Milano (Milano, Italy) for their help during the experimental tests as well as the Italian National Civil Protection Department which, through its Servizio Sismico Nazionale section, provided a scholarship. Also, the financial support of the Ministero dell'Istruzione, dell'Università e della Ricerca (MIUR) through the research programs 'Shape-memory alloys: constitutive modeling, structural analysis and design of innovative biomedical applications' and 'Shape-memory alloys: constitutive modeling, structural behaviour, experimental validation and applicability to innovative biomedical applications' is kindly acknowledged. Additional funding was provided by the Progetto Giovani Ricercatori—Anno 2002 of the Università degli Studi di Pavia (Pavia, Italy) and by the PECASE Program of the National Science Foundation under grant 0093868.

References

[1] Auricchio F and Sacco E 1997 A one-dimensional model for superelastic shape-memory alloys with different elastic properties between austenite and martensite *Int. J. Non-Linear Mech.* **32** 1101–14

[2] Auricchio F and Sacco E 1999 Modelling of the rate-dependent superelastic behavior of shape-memory alloys *Proc. Eur. Conf. on Comp. Mech. (München, Germany)*

[3] Auricchio F, Fugazza D and DesRoches R 2006 Rate-dependent thermo-mechanical modelling of superelastic shape-memory alloys for seismic applications *J. Intell. Mater. Syst. Struct.* at press

[4] Bernardini D and Brancaleoni F 1999 Shape memory alloys modelling for seismic applications *Proc. MANSIDE Project (Roma, Italy)* pp II 73–84

[5] Bernardini D and Vestroni F 2003 Non-isothermal oscillations of pseudoelastic devices *Int. J. Non-Linear Mech.* **38** 1297–313

[6] DesRoches R and Smith B 2004 Shape memory alloys in seismic resistant design and retrofit: a critical review of their potential and limitations *J. Earth. Eng.* **8** 415–29

[7] DesRoches R, McCormick J and Delemont M 2004 Cyclic properties of shape memory alloy wires and bars *J. Struct. Eng.* **130** 38–46

[8] Dolce M and Cardone D 2001 Mechanical behaviour of shape memory alloys for seismic applications 2. Austenite NiTi wires subjected to tension *Int. J. Mech. Sci.* **43** 2657–77

[9] Duerig T, Melton K, Stockel D and Wayman C 1990 *Engineering Aspects of Shape Memory Alloys* (London: Butterworth-Heinemann)

[10] Fugazza D 2005 Experimental investigation on the cyclic properties of superelastic NiTi shape-memory alloy wires and bars *Individual Study, European School for Advanced Studies in Reduction of Seismic Risk (Pavia, Italy)*

[11] Fugazza D, McCormick J, DesRoches R and Auricchio F 2004 Seismic analysis of a 3- and 6-story steel frame equipped with conventional and shape-memory alloy braces *Proc. US–Korea Joint Sem./Work. on Smart Str. Techn. (Seoul, Korea)*

[12] Graesser E J and Cozzarelli F A 1991 Shape-memory alloys as new materials for aseismic isolation *J. Eng. Mech.* **117** 2590–608

[13] Ikeda T, Nae F A, Naito H and Matsuzaki Y 2004 Constitutive model of shape memory alloys for unidirectional loading considering inner hysteresis loops *Smart Mater. Struct.* **13** 916–25

[14] Piedboeuf M C, Gauvin R and Thomas M 1998 Damping behavior of shape memory alloys: strain amplitude, frequency and temperature effects *J. Sound Vib.* **214** 885–901

[15] Saadat S, Salichs J, Noori M, Hou Z, Davoodi H, Bar-on I, Suzuki Y and Masuda A 2002 An overview of vibration and seismic applications of NiTi shape memory alloy *Smart Mater. Struct.* **11** 218–29

[16] Tamai H and Kitagawa Y 2002 Pseudoelastic behavior of shape memory alloy wire and its application to seismic resistance member for building *Comput. Mater. Sci.* **25** 218–27

[17] Wilde K, Gardoni P and Fujino Y 2000 Base isolation system with shape memory alloy device for elevated highway bridges *Eng. Struct.* **22** 222–9

[18] Wilson J C and Wesolowsky M J 2005 Shape memory alloys for seismic response modification: a state-of-the-art review *Earthquake Spectra* **21** 569–601